SCANNING VOL. 30, 287–298 (2008)
Published by Wiley Periodicals, Inc.†

Investigating the Optical Properties of Dislocations by Scanning Transmission Electron Microscopy

S. J. PENNYCOOK

Materials Science and Technology Division, Oak Ridge National Laboratory, Oak Ridge, Tennessee

Summary: The scanning transmission electron microscope (STEM) allows collection of a number of simultaneous signals, such as cathodoluminescence (CL), transmitted electron intensity and spectroscopic information from individual localized defects. This review traces the development of CL and atomic resolution imaging from their early inception through to the possibilities that exist today for achieving a true atomic-scale understanding of the optical properties of individual dislocations cores. This review is dedicated to Professor David Holt, a pioneer in this field. SCANNING 30: 287–298, 2008. Published 2008 by Wiley Periodicals, Inc.†

Key words: cathodoluminescence, dislocations, core structures, scanning transmission electron microscopy, electron energy loss spectroscopy, optical properties

PACS: 78.60.Hk, 61.72.Ff, 68.37.Lp, 68.37.Ma, 79.20.Uv

Introduction

Professor David Holt is widely recognized as one of the early pioneers in the development of the cathodoluminescence (CL) and electron beam-induced current (EBIC) modes of the scanning electron microscope (SEM) (Chase and Holt 1973; Datta *et al.* 1977; Davidson *et al.* 1975; Davidson and Rasul 1977; Dimitriadis *et al.* 1978; Holt and Chase 1973; Holt *et al.* 1973, 1974; Holt and Culpan 1970; Steyn *et al.* 1976; Williams and Yoffe 1968; Yacobi *et al.* 1977; Yacobi and Holt 1986, 1990). This work was an inspiration for the development of these modes for the scanning transmission electron microscope (STEM), especially for the present author during his thesis work (Pennycook 1978; Petroff and Lang 1977). This review covers the author's involvement in the early development of CL in the STEM, and in the subsequent ability to directly image dislocation core structures at atomic resolution through the Z-contrast or high-angle annular dark field (HAADF) mode of imaging. Today, with aberration-corrected microscopes, there exists an unprecedented potential to understand the optical emission and absorption properties of individual dislocation cores through CL and electron energy loss spectroscopy (EELS). Their optical properties could be correlated with their atomic structure, impurity content and electronic structure as determined from the combination of Z-contrast imaging and EELS at atomic resolution. Wide band gap optical materials such as the group III nitrides are currently under intense investigation for solid-state lighting and display applications, and dislocations are known to be nonradiative recombination centers in these materials (for an excellent review, see Humphreys 2008). Hence, the techniques pioneered by Professor Holt, coupled with theoretical investigations, could today be used to unravel the competing recombination mechanisms at dislocations, which could lead to new methods to enhance the radiative pathway and contribute to the enormous savings in energy use and greenhouse gas emissions expected with efficient solid-state lighting.

CL Studies of Dislocations

One of the key advantages of a scanning microscope is that any signal generated by the electron

†This work is a US government work and, as such, is in the public domain in the United States of America.

Address for reprints: S.J. Pennycook, Materials Science and Technology Division, Oak Ridge National Laboratory, Oak Ridge, TN 37831, E-mail: pennycooksj@ornl.gov

Received 2 May 2008; Accepted with revision 3 May 2008

DOI 10.1002/sca.20114
Published online 8 July 2008 in Wiley InterScience (www.interscience.wiley.com)

beam can, in principle, be collected and used to form an image. CL emitted by the specimen can be used to provide a map of optical emission intensity. Either the total emission can be used or, alternatively, with use of a spectrometer, particular spectral bands can be used for imaging. Such images give direct information on the spatial variation of optical properties. Most published work has involved semiconductor materials that emit light in the visible range, such as the III/V compound semiconductors and, more recently, particularly the nitride semiconductors. In this case, when viewed with band edge or near band edge emission, dislocations are seen dark if they act as nonradiative recombination centers or emit at wavelengths outside the range of detection. However, as has long been known, dislocations can also emit visible light at energies below the band gap (Datta *et al.* 1979; Kiflawi and Lang 1976; Myhajlenko *et al.* 1984; Piqueras *et al.* 1981). A particularly striking example of this effect is shown in Figure 1, where a line of hardness indents have been introduced into a MgO crystal, which was then cleaved so as to reveal the deformed region on two perpendicular surfaces (Pennycook 1978). In the secondary electron image only the indent itself is visible, but in the CL image the surrounding region is seen to emit strong luminescence. The three-dimensional structure of the slip bands induced by the indentation is apparent from the CL image, bands on the $\langle 1\,0\,0 \rangle$ and $\langle 1\,1\,0 \rangle$ planes being clearly seen. Notice, however, that the center of the indent does not emit strongly. High-voltage transmission electron microscopy (TEM) showed that such regions contained high densities of dislocations (Velednitskaya *et al.* 1975) and it was speculated that the luminescence in this region may be quenched. Evidence that this was the case came from the observation that the central region did emit strongly after thermal annealing which would reduce the defect density (Pennycook and Brown 1979). Later work showed that quenching occurred at levels of strain greater than around 5% (Brown *et al.* 1988).

Another example of luminescence emission from dislocations in a wide band gap material is the case of natural-type IIb diamond (Hanley *et al.* 1977; Kiflawi *et al.* 1976). In the SEM they show a network structure in CL as shown in Figure 2.

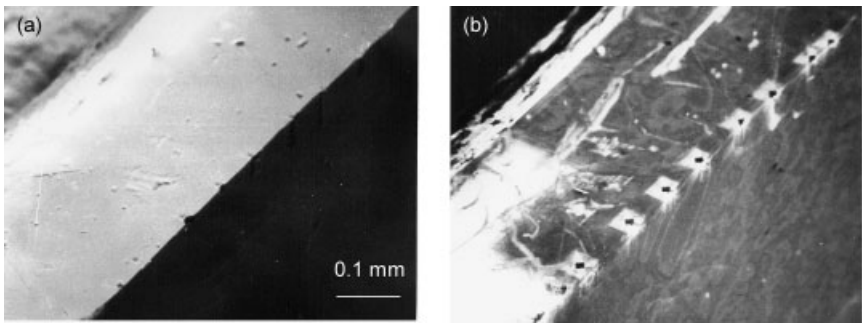

Fig 1. Comparison of (a) secondary electron and (b) CL images of an array of hardness indents in an MgO crystal, obtained in a Stereoscan S4-10 SEM. The crystal has been cleaved to reveal slip bands at 45° and 90° to the surface, which show bright optical emission. Reproduced from Pennycook (1978).

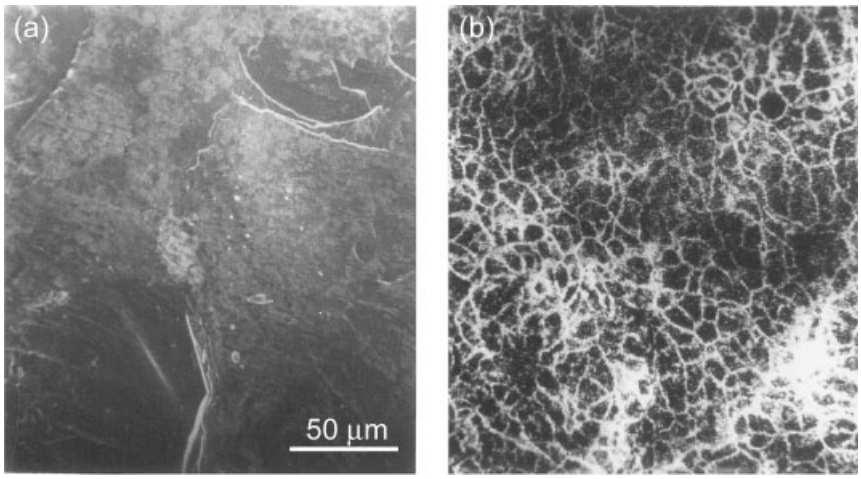

Fig 2. (a) Secondary electron and (b) CL images of a type IIb natural diamond showing a mosaic pattern of dislocations. Images obtained in a Stereoscan S4-10 SEM, reproduced from Pennycook (1978).

Individual dislocations within the cell walls are not resolved due to limited spatial resolution. CL in the STEM allows the potential for substantially enhanced spatial resolution, because the carrier diffusion length typically becomes limited to the order of the sample thickness since the surface of a thin sample is usually a strong nonradiative recombination pathway. The shorter diffusion length means higher spatial resolution is possible but at the expense of a reduction in total CL emission (Pennycook 1981), see Yuan *et al.* (1989) for a detailed discussion of the thickness dependence of CL emission. In addition, the most obvious benefit of STEM-CL is that the transmitted electron image is available for identification of the nature of the defects responsible (Petroff *et al.* 1980a,b, 1981). STEM-CL observations of dislocations in the type IIb diamond are shown in Figure 3, where individual dislocations are seen to be luminescent, but others are not, and no correlation was found with the dislocation Burgers' vector (Pennycook *et al.* 1980), see also Yamamoto *et al.* (1984).

A more recent example of STEM-CL is shown in Figure 4, showing a Eu-activated Y_2O_3 phosphor material grown by laser ablation (Gao *et al.* 2000). The structure is quite porous and a direct correlation was found between the size of the pores and luminescent efficiency. The pore size reduced both with slower deposition rate and with increased deposition temperature, resulting in increased

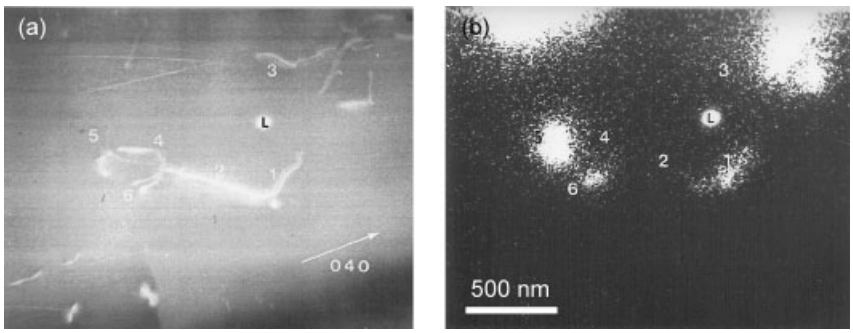

Fig 3. (a) Annular dark field and (b) CL images of dislocations in a type IIb natural diamond obtained in a VG Microscopes HB5 scanning transmission electron microscope. Dislocations 1 and 6 are luminescent, whereas dislocation 3 is not. Reproduced from Pennycook *et al.* (1980) with permission.

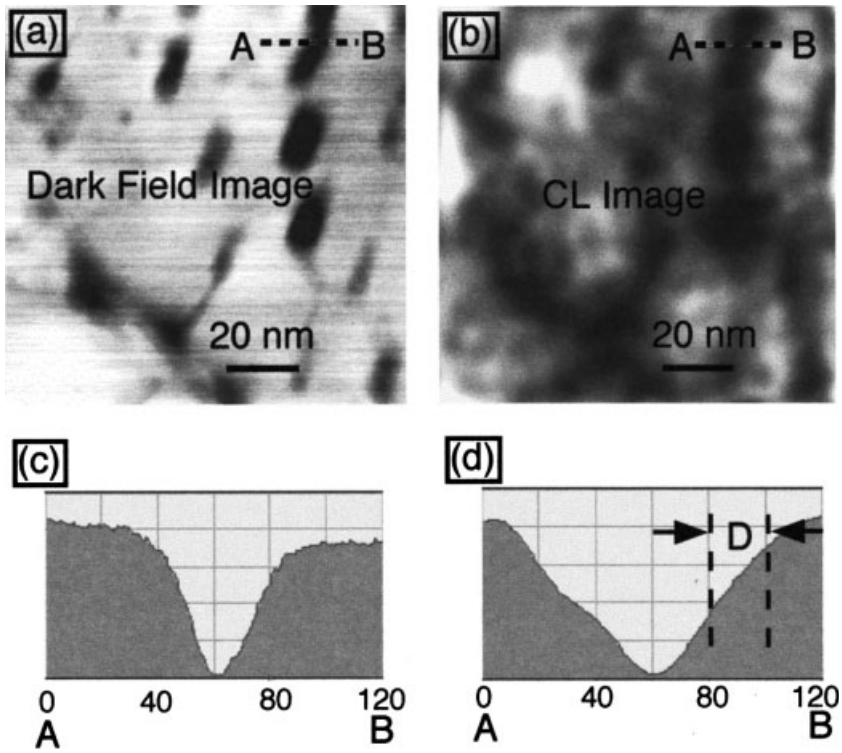

Fig 4. Correlation between (a) the ADF image and (b) the CL image of a porous Eu-activated Y_2O_3 phosphor. The corresponding line traces (c,d) show the existence of a dead layer around each pore, reproduced from Gao *et al.* (2000).

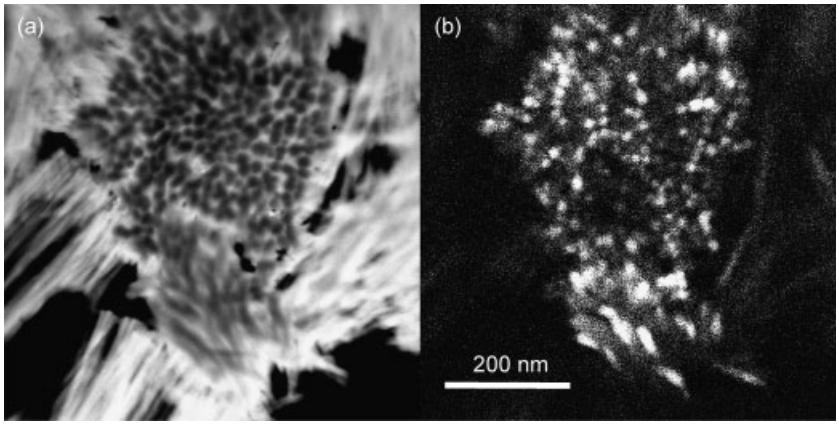

Fig 5. (a) Annular dark field and (b) CL images of ZnO nanorods recorded in a VG Microscopes HB501UX STEM, showing not all nanorods to be efficient light emitters, courtesy A. R. Lupini.

luminescence efficiency. The CL image clearly showed the origin of this effect to be due to the existence of a dead layer surrounding each pore, as seen in Figure 4. The ADF image shows a pore size of 10 nm, which is effectively doubled in the CL image because of the dead layer. Taking account of this increased volume of nonradiative material accounted for the decreased luminescence efficiency in the porous materials.

A topical example of the potential for CL in the nanoscience era is the case of ZnO that can be grown in the form of vertically aligned arrays of nanorods, each with a quantum well structure grown on their tip (Park *et al.* 2002, 2003). Although the photoluminescence spectrum showed clear quantum confinement effects, STEM-CL imaging showed that, in fact, not all the nanorods were efficient light emitters (Fig. 5). The source of the quenched luminescence could possibly be due to dislocations but that could not be confirmed in this study.

In recent years most CL work has focused on the nitrides, using bulk samples in the SEM, see, for example, Chichibu *et al.* (2007), Choi *et al.* (2004), Dassonneville *et al.* (2001), Gustafsson (2006), Kwon *et al.* (2008), Pauc *et al.* (2006), Ponce *et al.* (2003) and Zaldivar *et al.* (1998). Identification of dislocations as sources of nonradiative recombination has been by comparison to transmitted electron images taken in the TEM or STEM, (Albrecht *et al.* 2002; Cherns *et al.* 2001; Lakner et al. 1988; Ponce *et al.* 1996, 2003; Strunk *et al.* 2006; Yamamoto *et al.* 2003). Other methods also exist for local mapping of luminescence, for example the scanning near-field optical microscope or the scanning tunneling microscope, see Gustafsson *et al.* (1998) for a review of these techniques.

In all these situations the dislocations are introducing energy levels in the band gap that are facilitating radiative or nonradiative recombination of electron–hole pairs. The mechanism could involve intrinsic electronic states due for example to dangling bonds at the dislocation cores, or alternatively could be due to impurities segregated to the highly strained region of the core. In principle, these mid-gap levels could be seen in EELS, which involves excitation of electrons from the valence band into the (unoccupied) states in the band gap (Gutierrez-Sosa *et al.* 2002; Pennycook 1981). Also, in principle, the presence of impurities could be determined from EELS, although the sensitivity in these early studies was not sufficient. To understand dislocation optical properties at the most fundamental level requires the atomic arrangements and impurity sites at the core of the defect to be determined, defect by defect. Then, through first principles theoretical studies the optical transitions could be calculated and the origin of the electronic and optical properties would be revealed. Differences between benign defects (if any) and defects showing strong carrier recombination would indicate directions for process development toward more efficient devices. With the benefit of hindsight it is clear that this alluring possibility needed to wait for the development of smaller electron probes.

Direct Imaging of Dislocation Core Structures

The imaging of dislocations in the TEM began through diffraction contrast, tilting a sample close to a Bragg reflection such that any local crystal rotations (due for example to a dislocation strain field) would change the diffracted intensity (Bollmann, 1956; Hirsch *et al.* 1956). In the very same year, it was also demonstrated that two diffracted beams could be passed simultaneously through the microscope objective lens to form interference

fringes, or lattice fringes, the first representative image of a crystal lattice. Over the years the resolution gradually improved and the contrast mechanisms became well understood, for reviews of these developments, see Smith (1997, 2008). Correlating the image to atomic positions is not always simple since the relative phases of the diffracted beams depend on the thickness and microscope focus and aberrations, so the imaging of dislocation core structures relied on extensive image simulations, at least until the recent introduction of aberration correctors (Kisielowski *et al.* 2006).

It was the STEM that produced the first images of individual atoms, heavy atoms supported on a thin carbon film (Crewe *et al.* 1970; Isaacson *et al.* 1977), also images of small U nanocrystals were obtained (Wall *et al.* 1974). Owing to the strong atomic number (Z) contrast in annular dark field (ADF) images, single atoms of different Z could even be distinguished just from their relative intensities (Isaacson *et al.* 1979). The lack of phase contrast effects in the image was consistent with the image being incoherent in nature, like that of a camera. Atoms always showed bright contrast, never reversed contrast. These advantages were seen also in image simulations (Engel *et al.* 1974), and in addition the simulations confirmed the enhanced resolution expected for an incoherent image compared with a phase contrast image (Born and Wolf 1980). These advantages were subsequently demonstrated for thin crystals by Cowley (1979).

Significant questions still remained, however, over the degree of incoherence of ADF images (Ade 1977; Cowley 1975, 1976), particularly for atoms having the same projected position in the transverse plane but different heights along the beam direction (e.g., columns of atoms). It was clear that the intensity in this case did not rise linearly with the number of atoms as it should if all atoms contributed equally. Furthermore, it was felt that the apparent incoherent characteristics could apply only for extremely thin crystals and would not hold for the typical thicknesses used for materials research in which strong dynamical diffraction effects would certainly be present. Dynamical diffraction causes contrast reversals in phase contrast imaging. It was the introduction of the high-angle detector that enabled the widespread adoption of incoherent Z-contrast imaging. Suggested by Treacy *et al.* (1978) as a possible means to suppress diffraction contrast effects in the imaging of catalyst clusters, and to improve their contrast, it was subsequently shown to be highly effective (Treacy 1981, 1982; Treacy *et al.* 1980). Later, a high-angle detector was used to image dopant profiles in semiconductors (Pennycook *et al.* 1986; Pennycook and Narayan 1984) and the prediction was made that for a probe of atomic dimensions the high-angle detector would give a direct, incoherent image of materials. To quote from Pennycook *et al.* (1986) "In thin samples of crystalline materials, atomic resolution Z-contrast imaging seems entirely feasible and entirely complementary to conventional high resolution structure imaging." With the introduction of a commercially available STEM with a (theoretical) probe size of 2.2 Å at 100 kV (not including any source contribution) this prediction proved correct (Pennycook and Boatner 1988) and led to the surprising discovery that the HAADF image did not in fact show dynamical oscillations with increasing specimen thickness (Pennycook 1989). It behaved like a true incoherent image at all thicknesses, although the intensity was indeed not linear with thickness, rising rapidly initially and then saturating and gaining an increasing background intensity.

The explanation proposed for this effect was that the high angle scattering is generated close to the atomic nuclei, i.e. it is essentially Rutherford scattering, hence the strong Z-contrast. Owing to thermal vibrations it is generated incoherently from each atom site in proportion to the electron intensity in the vicinity of each nucleus. This explained the absence of dynamical oscillations. The electron intensity in this region of the unit cell is dominated by 1s-type Bloch states (Pennycook and Jesson 1990, 1991, 1992); the 2s Bloch states that cause the thickness oscillations in phase contrast images have only a small amplitude. Hence, tuning the detector angle effectively stops the interference between the two dominant Bloch states excited around each atomic column. Therefore, the tendency of the beam to focus onto the atomic columns and channel along them until scattered to high angles explained the thickness dependence of the image intensity. Further investigation revealed that the wide angular range of the HAADF detector effectively produced an incoherent image just by averaging over the diffraction pattern (Jesson and Pennycook 1993), so that even with coherent scattering the image would show incoherent characteristics in the transverse plane, free from contrast reversals and with enhanced resolution just like the early Z-contrast results. The incoherent characteristics would even remain with thick crystals under dynamical conditions (Nellist and Pennycook 1999). The role of the thermal vibrations was to break the coherence in the beam direction (Jesson and Pennycook 1995), converting an oscillatory thickness dependence for pure coherent scattering into the monotonically increasing intensity seen experimentally. For more analysis of HAADF image formation, see Allen *et al.* (2003), Amali and Rez (1997), Dwyer and Etheridge (2003), Findlay *et al.* (2003), Hillyard *et al.* (1993), Hillyard and Silcox (1993, 1995),

Ishizuka (2001), Kirkland (1998), Mobus and Nufer (2003), Nellist and Pennycook (2000), Peng *et al.* (2004), Pennycook and Nellist (1999) and Rafferty *et al.* (2001).

These incoherent characteristics were of great value in imaging atomic arrangements at interfaces and dislocation cores, largely avoiding the need to simulate images using trial structures. Even in highly strained regions the atomic positions could generally be determined directly from the image, with sufficient precision to allow theoretical modeling of the structure. In many cases new and unpredicted structures were found, for some early examples, see Browning *et al.* (2001), Chisholm *et al.* (1994a,b, 1998), Chisholm and Pennycook (1997), Dickey *et al.* (1997, 1998), James *et al.* (1998), Jesson *et al.* (1991, 1993, 1995), Lakner et al. (1996) Muller *et al.* (1998), Pennycook *et al.* (1996) and Yan *et al.* (1998).

It was also soon realized that similar advantages should apply with EELS, which can be performed simultaneously with the HAADF image using an axial spectrometer to energy filter electrons passing through the hole in the annular detector (Crewe and Wall, 1970). Atomic resolution EELS was demonstrated in 1993 using a $CoSi_2$/Si interface (Browning *et al.*, 1993), and it was observed that the Co core loss intensity drop abruptly between the last plane of the silicide and the first plane of the silicon. In these experiments the beam was scanned parallel to the interface during acquisition of the EELS data to avoid beam damage. The scanning also allowed the beam to be accurately located over the selected plane by monitoring the HAADF detector intensity throughout spectrum acquisition. In later work, with more damage-resistant materials, true column-by-column EELS was possible. Figure 6(a) shows an image of a $SrTiO_3$ grain boundary taken in a 300 kV STEM (theoretical probe size 1.3 Å) in which the boundary is seen to comprise a repeating array of structural units (Duscher *et al.* 1998). The surprising result found in this system was that dislocation core structures were more complex than previously supposed, comprising two (or three) like ion atomic columns in a pentagonal framework of the other cation (McGibbon *et al.* 1994). In the case of the $36^\circ\langle 0\,0\,1\rangle$ tilt grain boundary of Figure 6, Sr and Ti centered cores alternate along the boundary plane. The identical structure was seen in all regions of the bicrystal grain boundary. Investigation of other misorientations showed that the structural unit sequence closely followed the predictions of the structural unit model (Sutton 1988; Sutton and Vitek 1983), provided the more complex structure was taken into account (Browning *et al.* 1995; McGibbon *et al.* 1996).

Figure 6(b) shows EELS data (collected on the 100 kV STEM) from different columns. It is seen that not only is the intensity of the various edges different from column to column, but also the fine structure on the edge changes indicating a different local electronic structure. In this particular example the presence of Mn dopant is seen in the EELS, and clearly is preferentially segregated to the dislocation core containing Ti atoms (site 2), at a concentration higher than in the nearby "bulk" column 1, whereas the Mn concentration in the Sr core 3 is lower (or may actually be absent). Furthermore, insight into the impurity valence state can be obtained by examining the ratio of the Mn L3 and L2 peaks, and comparing with standard samples (Kurata and Colliex 1993). The Mn is found to be closer to a+3 valence than the +4 valence expected in a fully stoichiometric boundary structure.

With the successful correction of lens aberrations (Haider et al. 1998; Batson et al. 2002) the sensitivity

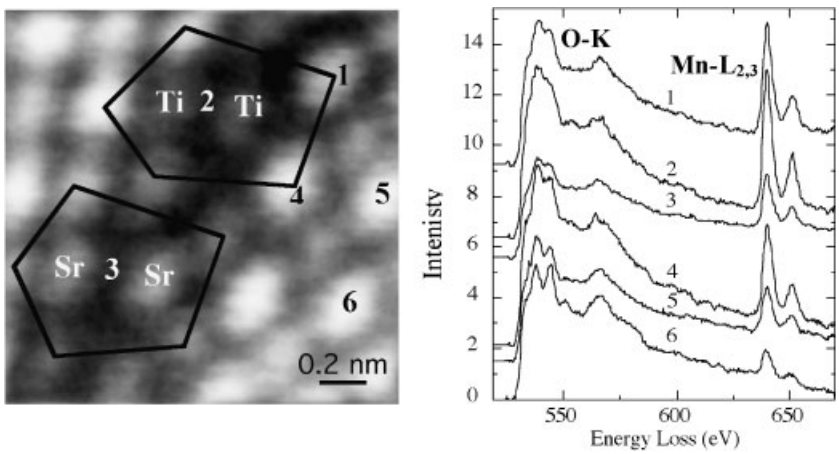

Fig 6. (a) Z-contrast image from a Mn-doped 36° $SrTiO_3$ grain boundary recorded on a 300 kV STEM. (b) EELS spectra recorded in a 100 kV STEM by stopping the probe on the corresponding atomic columns, revealing differences in Mn concentration and valence at different sites. Reproduced from Duscher *et al.* (1998).

of EELS has been greatly increased, more of the incident probe being focused on the column of interest and less illuminating neighboring columns. This has allowed the first spectroscopic identification of an individual impurity atom in a single atomic column (Varela *et al.* 2004), and the first true two-dimensional EELS maps showing atomic resolution (Bosman *et al.* 2007).

Correlating Atomic Structure to Properties Through Theory

Here we show a few case studies of grain boundaries where the local atomic and electronic structure indicated by STEM has been linked to macroscopic properties though density-functional theory. For a more extended review on dislocations, see Chisholm and Pennycook (2006). As grain boundaries are nothing more than arrays of dislocation cores, the same approach could in future be fruitfully applied to understand optical properties of individual dislocation cores or grain boundaries in materials.

The combination of the image with the spectroscopy shown in Figure 6 provides a wealth of data, but not an explanation of the properties of the boundaries, which can be electrically active, finding use in varistors and capacitors. Phenomenologically, such grain boundaries are assumed to be charged, but there was no microscopic explanation for the origin of such a charge (Taylor *et al.* 1952; Vollman and Waser 1994). Therefore, to explain the properties, first principles density-functional calculations were carried out, both to refine and validate the models suggested from the images by determining the lowest energy arrangements that were consistent with the images, and also to explain the origin of the band-bending and electrical activity (Kim *et al.* 2001). In both types of core, nonstoichiometry was found to be energetically favorable; in the Sr-centered core, two half-columns of Sr were favored, whereas in the Ti-centered cores, full Ti columns were favored, and in both cases O vacancy segregation energies were of several electron volts, implying that the boundaries would be O deficient. This would be consistent with the EELS indications of a reduced Mn oxidation state in the boundary.

O deficiency also provides a microscopic explanation for the electrical activity, often described as double Schottky barriers. The Ti or Mn cations that are in a+3 oxidation state compared with bulk will have one excess electron. In the theoretical calculation this electron sits in the conduction band, spatially located around the cation, as shown in Figure 7, and the Fermi level is also in the conduction band. In the real material, however, the unpaired electron will migrate from the boundary to

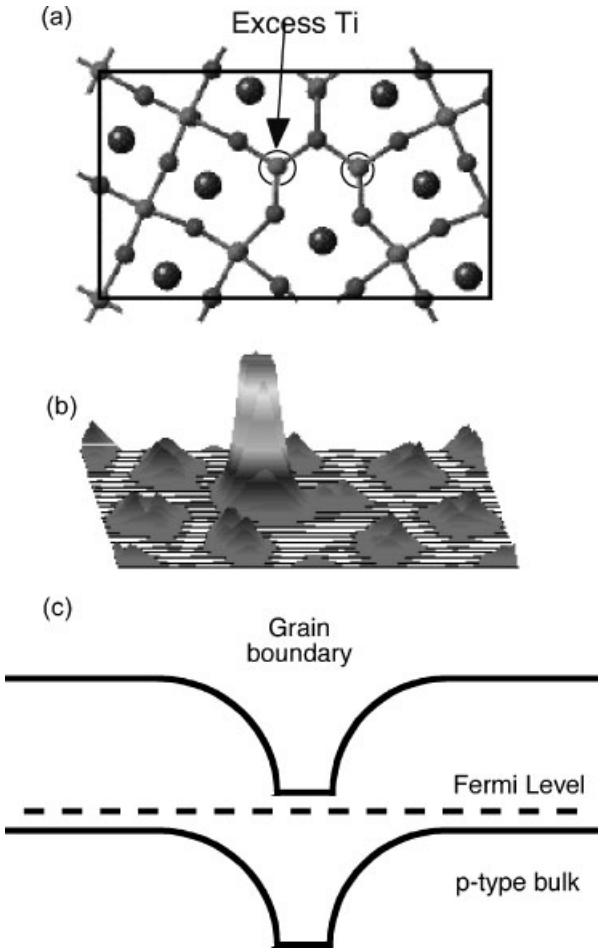

Fig 7. (a) Schematic structure of one unit cell of a 53° grain boundary in $SrTiO_3$, with one column in the Ti-centered core containing excess Ti. (b) A plot of the charge density in the conduction band showing an accumulation over the non-stoichiometric Ti column. (c) Schematic of the band bending established with the grain boudary embedded in p-type bulk material. Adapted from Kim *et al.* (2001).

acceptor impurity states that are present in the actual p-type bulk $SrTiO_3$ but not included in the theoretical calculation. In the p-type bulk the Fermi level lies within the acceptor band, close to the valence band. When the electron leaves the grain boundary, which saves an energy per electron close to the band gap energy, it sets up a space charge around the grain boundary and the bands will bend in order to keep the Fermi level flat, as shown in the schematic (Kim *et al.* 2001). This is the microscopic origin of the double Schottky barrier.

The high-temperature superconductor, $YBa_2Cu_3O_{7-x}$ (YBCO), has a structure closely related to the perovskite structure, and grain boundaries show structural units and sequences exactly as predicted by analogy with $SrTiO_3$ where the Sr column is replaced with a mixed Y/Ba column and Ti by Cu. These materials are hole doped for optimum O content (x near zero). Very soon after these

materials were discovered it was found that grain boundaries caused an enormous decrease in critical current. Studies using bicrystals showed an exponential reduction in grain boundary critical current with misorientation (Chaudhari *et al.* 1988; Dimos *et al.* 1988 1990). By analogy with the situation in $SrTiO_3$ assuming the grain boundary to be O deficient would make the dislocation cores charged. The resultant band bending would create a hole depletion zone and its width could be predicted quantitatively from the structural unit model. The expected width of the depletion zone was found to increase linearly with grain boundary misorientation. As the supercurrent is forced to tunnel through this non-superconducting zone at the grain boundary this result naturally explained the exponential reduction in critical current (Browning *et al.* 1998 1999). More recently with aberration-corrected STEM imaging and column-by-column EELS have shown the differences between Ca-doped and undoped grain boundaries and in conjunction with theory have explained how Ca doping improves the grain boundary critical current (Klie *et al.* 2005). The results again show how complex such effects can be. It was previously assumed that Ca would segregate for Y at the grain boundary as it is known to do in the bulk which since Ca is +2 and Y is +3 was thought would donate holes to the grain boundary and compensate the intrinsic hole depletion. However in the highly strained region of the dislocation core new effects were found. Ca substituted for Ba in regions of compression and for Cu in regions of tension because in those sites the local stresses could be reduced. By reducing the stresses the driving force for the O depletion was reduced and indeed O concentrations were seen to increase to bulk values at most of the sites. Theory also predicted that O vacancy formation energies would be restored to near bulk values. Hence the picture emerged of a co-operative doping phenomenon driven by the large strain fields of the dislocation core.

Future Directions

A significant body of work in STEM EELS and theory already exists in the nitride semiconductors. Atomic arrangements at dislocation cores have been imaged as shown in Figure 8 where an eightfold arrangement of atomic columns is seen at the core of a dislocation representing the termination of two additional planes present above the core (Xin *et al.* 1998). Such dislocations have edge character and the atomic coordinates can be accurately extracted by maximum entropy processing. The eight-fold arrangement was consistent with prior theoretical predictions in this case (Elsner *et al.* 1997). Later work showed such images to be characteristic of perfect edge dislocations mixed dislocations showing a blurring of the columns near the core (Xin *et al.* 2000b). Pure screw dislocation cores can also be located because of the strain field they generate where they intersect the sample surface which for moderate inner detector angles gives contrast in the ADF image as shown in Figure 9. EELS has also shown changes in the electronic structure at dislocations cores (Arslan and Browning 2002; Xin *et al.* 2000a) and the segregation of O to the core region in amounts depending on the nature of the core (Arslan and Browning 2003; Brockt and Lakner 2000).

There have also been many CL studies directly implicating dislocation cores as nonradiative recombination centers (Albrecht *et al.* 2002; Cherns *et al.* 2001; Ponce *et al.* 1996 2003; Strunk *et al.* 2006; Yamamoto *et al.* 2003). However it seems that many fundamental questions remain. Do all defects of the same type behave the same? Or does radiative

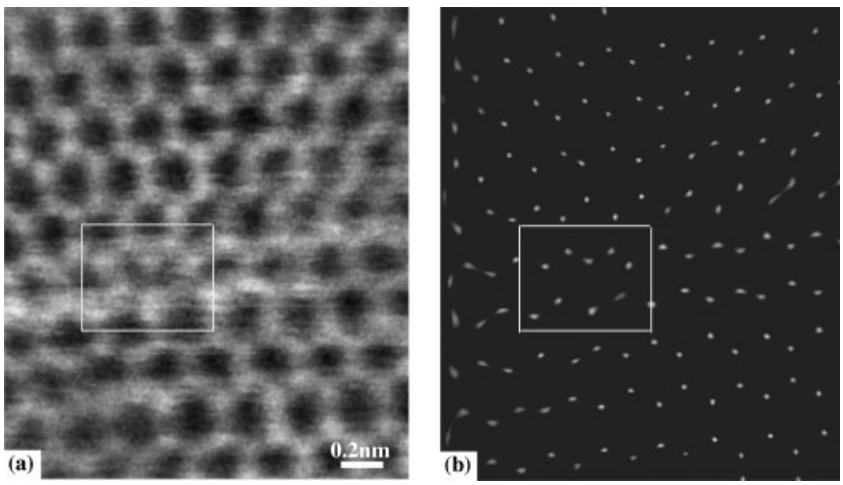

Fig 8. (a) Z-contrast image of a pure edge dislocation core in GaN and (b) a maximum entropy reconstruction showing the eightfold arrangement of atomic columns at the core, reproduced from Xin *et al.* (1998).

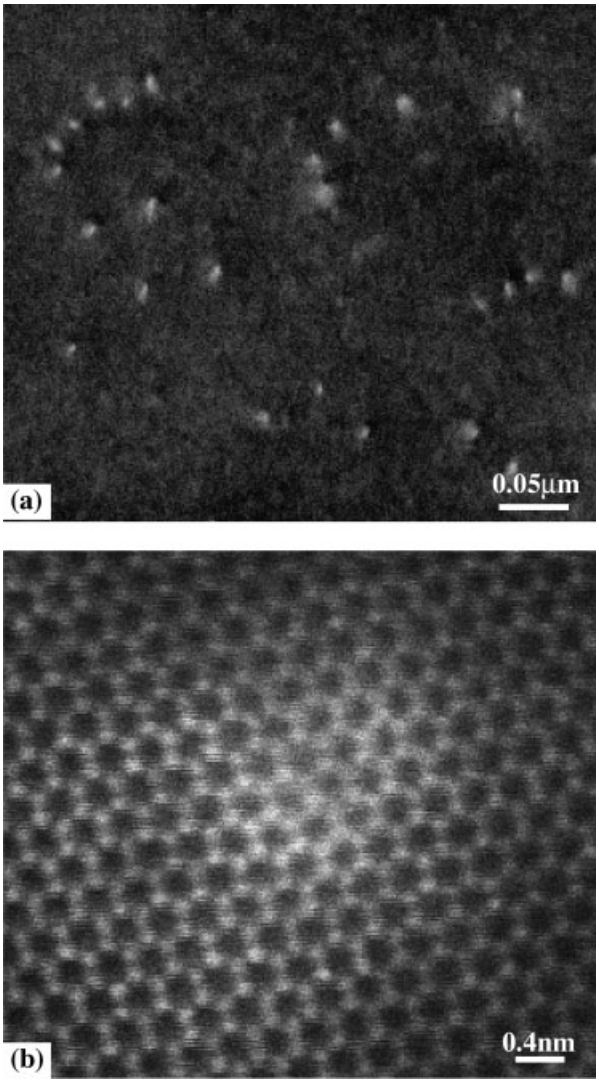

Fig 9. (a) Low magnification ADF image of threading dislocations in GaN visible via strain contrast. (b) Atomic-resolution image of the core of a pure screw dislocation. Images reproduced from Xin *et al*. (1998).

or nonradiative efficiency depend on local impurity content such as O concentration? An atomic-level understanding of the optical properties of dislocations remains to be achieved and it would seem that the incorporation of a CL or EBIC detection system into an aberration-corrected STEM could provide a significant advance toward achieving such understanding which surely would represent the ultimate development of the techniques pioneered by Prof. David Holt.

Acknowledgements

S. J. P. acknowledges his collaborators for the work reviewed here L. M. Brown A. J. Craven H. J. Gao G. Duscher M. Kim D. Kumar K. G. Cho R. K. Singh A. R. Lupini M. Kim N. D. Browning K. Sohlberg S. T. Pantelides S. Rujirawat S. Sivananthan Y. P. Chen and P. D. Nellist and acknowledges support from the Division of Materials Sciences and Engineering US Department of Energy.

References

Ade G: Incoherent imaging in scanning-transmission electron-microscope (STEM). *Optik* **49** 113–116 (1977).

Albrecht M Strunk HP Weyher JL Grzegory I Porowski S *et al*: Carrier recombination at single dislocations in GaN measured by cathodoluminescence in a transmission electron microscope. *J Appl Phys* **92** 2000–2005 (2002).

Allen LJ Findlay SD Oxley MP Rossouw CJ: Lattice-resolution contrast from a focused coherent electron probe. Part I. *Ultramicroscopy* **96** 47–63 (2003).

Amali A Rez P: Theory of lattice resolution in high-angle annular dark-field images. *Microsc Microanal* **3** 28–46 (1997).

Arslan I Browning ND: Intrinsic electronic structure of threading dislocations in GaN. *Phys Rev B* **65** Art. No. 075310 (2002).

Arslan I Browning ND: Role of oxygen at screw dislocations in GaN. *Phys Rev Lett* **91** Art. No. 165501 (2003).

Batson PE Dellby N Krivanek OL: Sub-angstrom resolution using aberration corrected electron optics. *Nature* **418** 617–620 (2002).

Bollmann W. Interference effects in the electron microscopy of thin crystal foils. *Phys Rev* **103** 1588 (1956).

Born M Wolf E: Principles of Optics. Pergamon Press,UK (1980).

Bosman M Keast VJ Garcia-Munoz JL D'Alfonso AJ Findlay SD *et al*: Two-dimensional mapping of chemical information at atomic resolution. *Phys Rev Lett* **99** Art. No. 086102 (2007).

Brockt G Lakner H: Nanoscale EELS analysis of dielectric function and bandgap properties in GaN and related materials. *Micron* **31** 435–440 (2000).

Brown LM Khan MY Chaudhri MM: Quenching of cathodoluminescence at the center of hardness indentations on a (100) face of MgO. *Philos Mag A* **57** 187–196 (1988).

Browning ND Arslan I Ito Y James EM Klie RF *et al*: Application of atomic scale STEM techniques to the study of interfaces and defects in materials. *J. Electron Microsc* **50** 205–218 (2001).

Browning ND Buban JP Nellist PD Norton DP Chisholm MF *et al*: The atomic origins of reduced critical currents at 001 tilt grain boundaries in $YBa_2Cu_3O_{7-\delta}$ thin films. *Physica C* **294** 183–193 (1998).

Browning ND Buban JP Prouteau C Duscher G Pennycook SJ: Investigating the atomic scale structure and chemistry of grain boundaries in high-T_c superconductors. *Micron* **30** 425–436 (1999).

Browning ND Chisholm MF Pennycook SJ: Atomic-resolution chemical-analysis using a scanning-transmission electron-microscope. *Nature* **366** 143–146 (1993).

Browning ND Pennycook SJ Chisholm MF McGibbon MM McGibbon AJ: Observation of structural units at symmetric [001] tilt boundaries in $SrTiO_3$. *Interface Sci* **2** 397–423 (1995).

Chase BD Holt DB: Scanning electron-microscope studies of electroluminescent diodes of GaAs and GaP.1. Micrographic observations. *Phys Status Solidi A* **19** 467–478 (1973).

Chaudhari P Mannhart J Dimos D Tsuei CC Chi J *et al*: Direct measurement of the superconducting properties of

single grain-boundaries in $YBa_2Cu_3O_7$-^{TM}. *Phys Rev Lett* **60** 1653–1656 (1988).

Cherns D Henley SJ Ponce FA: Edge and screw dislocations as nonradiative centers in InGaN/GaN quantum well luminescence. *Appl Phys Lett* **78** 2691–2693 (2001).

Chichibu SF Onuma T Hashimoto T Fujito K Wu F *et al*: Impacts of dislocation bending and impurity incorporation on the local cathodoluminescence spectra of GaN grown by ammonothermal method. *Appl Phys Lett* **91** Art. No. 251911 (2007).

Chisholm MF Browning ND Pennycook SJ Jebasinski R Mantl S: Z-contrast investigation of the ordered atomic interface of $CoSi_2$/Si(001) layers. *Appl Phys Lett* **64** 3608–3610 (1994a).

Chisholm MF Maiti A Pennycook SJ Pantelides ST: Atomic configurations and energetics of arsenic impurities in a silicon grain boundary. *Phys Rev Lett* **81** 132–135 (1998).

Chisholm MF Pennycook SJ: Z-contrast imaging of grain-boundary core structures in semiconductors. *MRS Bull* **22** 53–57 (1997).

Chisholm MF Pennycook SJ: Direct imaging of dislocation core structures by Z-contrast STEM. *Philos Mag* **86** 4699–4725 (2006).

Chisholm MF Pennycook SJ Jebasinski R Mantl S: New interface structure for A-type $CoSi_2$/Si(111). *Appl Phys Lett* **64** 2409–2411 (1994b).

Choi YS Park JH Kim SS Song HJ Lee SH *et al*: Effects of dislocations on the luminescence of GaN/InGaN multi-quantum-well light-emitting-diode layers. *Mater Lett* **58** 2614–2617 (2004).

Cowley JM: Coherent and incoherent imaging in scanning-transmission electron-microscope. *J Phys D* **8** L77–L79 (1975).

Cowley JM: Scanning-transmission electron-microscopy of thin specimens. *Ultramicroscopy* **2** 3–16 (1976).

Cowley JM: High-resolution studies of crystals using STEM. *Chem Scr* **14** 33–38 (1979).

Crewe AV Wall J: A Scanning microscope with 5 Å resolution. *J Mol Biol* **48** 375 (1970).

Crewe AV Wall J Langmore J: Visibility of single atoms. *Science* **168** 1338–1340 (1970).

Dassonneville S Amokrane A Sieber B Farvacque JL Beaumont B *et al*: Luminescence of epitaxial GaN laterally overgrown on (0001) sapphire substrate: spectroscopic characterization and dislocation contrasts. *J Appl Phys* **89** 3736–3743 (2001).

Datta S Boswarva IM Holt DB: Cathodoluminescence in deformed MgO crystals. *J Phys Chem Solids* **40** 567–571 (1979).

Datta S Yacobi BG Holt DB: Scanning electron-microscope studies of local variations in cathodoluminescence in striated ZnS platelets. *J Mater Sci* **12** 2411–2420 (1977).

Davidson SM Iqbal MZ Northrop DC: SEM cathodeluminescent studies of plastically deformed gallium-phosphide. *Phys Status Solidi A* **29** 571–578 (1975).

Davidson SM Rasul A: High-resolution cathodoluminescence analysis system. *J Phys E* **10**:43–46 (1977).

Dickey EC Dravid VP Nellist PD Wallis DJ Pennycook SJ *et al*: Structure and bonding at Ni–ZrO_2 (cubic) interfaces formed by the reduction of a NiO–ZrO_2 (cubic) composite. *Microsc Microanal* **3** 443–450 (1997).

Dickey EC Dravid VP Nellist PD Wallis DJ Pennycook SJ: Three-dimensional atomic structure of NiO–ZrO_2 (cubic) interfaces. *Acta Mater* **46** 1801–1816 (1998).

Dimitriadis CA Huang E Davidson SM: SEM cathodoluminescence studies of dislocation recombination in GaP. *Solid State Electron* **21** 1419–1423 (1978).

Dimos D Chaudhari P Mannhart J: Superconducting transport-properties of grain-boundaries in $YBa_2Cu_3O_7$ bicrystals. *Phys Rev B* **41** 4038–4049 (1990).

Dimos D Chaudhari P Mannhart J Legoues FK: Orientation dependence of grain-boundary critical currents in $YBa_2Cu_3O_7$-^{TM} bicrystals. *Phys Rev Lett* **61** 219–222 (1988).

Duscher G Browning ND Pennycook SJ: Atomic column resolved electron energy-loss spectroscopy. *Phys Status Solidi A* **166** 327–342 (1998).

Dwyer C Etheridge J: Scattering of Å-scale electron probes in silicon. *Ultramicroscopy* **96** 343 (2003).

Elsner J Jones R Sitch PK Porezag VD Elstner M *et al*: Theory of threading edge and screw dislocations in GaN. *Phys Rev Lett* **79** 3672–3675 (1997).

Engel A Wiggins JW Woodruff DC: Comparison of calculated images generated by 6 modes of transmission electron-microscopy. *J Appl Phys* **45** 2739–2747 (1974).

Findlay SD Allen LJ Oxley MP Rossouw CJ: Lattice-resolution contrast from a focused coherent electron probe. Part II. *Ultramicroscopy* **96** 65–81 (2003).

Gao HJ Duscher G Kim M Pennycook SJ Kumar D *et al*: Cathodoluminescent properties at nanometer resolution through Z-contrast scanning transmission electron microscopy. *Appl Phys Lett* **77** 594–596 (2000).

Gustafsson A: Cathodoluminescence studies of nanostructured semiconductors. *J Microsc-Oxford* **224** 72–78 (2006).

Gustafsson A Pistol ME Montelius L Samuelson L: Local probe techniques for luminescence studies of low-dimensional semiconductor structures. *J Appl Phys* **84** 1715–1775 (1998).

Gutierrez-Sosa A Bangert U Harvey AJ Fall CJ Jones R *et al*: Band-gap-related energies of threading dislocations and quantum wells in group-III nitride films as derived from electron energy loss spectroscopy. *Phys Rev B* **66** (2002).

Haider M Uhlemann S Schwan E Rose H Kabius B Urban K: Electron microscopy image enhanced. *Nature* **392** 768–769 (1998).

Hanley PL Kiflawi I Lang AR: Topographically identifiable sources of cathodoluminescence in natural diamonds. *Philos Trans R Soc London Ser A* **284** 330–368 (1977).

Hillyard S Loane RF Silcox J: Annular dark-field imaging—resolution and thickness effects. *Ultramicroscopy* **49** 14–25 (1993).

Hillyard S Silcox J: Thickness effects in ADF STEM zone-axis images. *Ultramicroscopy* **52** 325–334 (1993).

Hillyard S Silcox J: Detector geometry thermal diffuse-scattering and strain effects in ADF STEM imaging. *Ultramicroscopy* **58** 6–17 (1995).

Hirsch PB Horne RW Whelan MJ: Direct observations of the arrangement and motion of dislocations in aluminium. *Philos Mag* **1** 677–684 (1956).

Holt DB Chase BD: Scanning electron-microscope studies of electroluminescent diodes of GaAs and GaP. 2. Analysis of GaAs line scan traces. *Phys Status Solidi A* **20** 135–144 (1973).

Holt DB Chase BD Censlive M: Scanning electron-microscope studies of electroluminescent diodes of GaAs and GaP. 3. Quantitative line scan observations on GaP. *Phys Status Solidi A* **20** 459–467 (1973).

Holt DB Culpan M: Scanning electron microscope studies of striations in ZnS. *J Mater Sci* **5** 546 (1970).

Holt DB Muir MD Grant PR Boswarva IM: In Quantitative Scanning Electron Microscopy. Academic Press 213–286 (1974).

Humphreys CJ: Solid-state lighting. *MRS Bull* **33** 459–477 (2008).

Isaacson M Kopf D Ohtsuki M Utlaut M: Atomic imaging using the dark-field annular detector in the STEM. *Ultramicroscopy* **4** 101–104 (1979).

Isaacson M Kopf D Utlaut M Parker NW Crewe AV: Direct observations of atomic diffusion by scanning-transmission electron-microscopy. *Proc Natl Acad Sci USA* **74** 1802–1806 (1977).

Ishizuka K: Prospects of atomic resolution imaging with an aberration-corrected STEM. *J Electron Microsc* **50** 291–305 (2001).

James EM Browning ND Nicholls AW Kawasaki M Xin Y *et al*: Demonstration of atomic resolution Z-contrast imaging by a JEOL JEM-2010F scanning transmission electron microscope. *J Electron Microsc* **47** 561–574 (1998).

Jesson DE Pennycook SJ Baribeau JM: Direct imaging of interfacial ordering in ultrathin $(Si_mGe_n)_P$ superlattices. *Phys Rev Lett* **66** 750–753 (1991).

Jesson DE Pennycook SJ Baribeau JM Houghton DC: Direct imaging of surface cusp evolution during strained-layer epitaxy and implications for strain relaxation. *Phys Rev Lett* **71** 1744–1747 (1993).

Jesson DE Pennycook SJ: Incoherent imaging of thin specimens using coherently scattered electrons. *Proc R Soc London A* **441** 261–281 (1993).

Jesson DE Pennycook SJ: Incoherent imaging of crystals using thermally scattered electrons. *Proc R Soc London A* **449** 273–293 (1995).

Kiflawi I Lang AR: Correspondence between cathodoluminescence images and x-ray-diffraction contrast images of individual dislocations in diamond. *Philos Mag* **33** 697–701 (1976).

Kim M Duscher G Browning ND Sohlberg K Pantelides ST *et al*: Nonstoichiometry and the electrical activity of grain boundaries in $SrTiO_3$. *Phys Rev Lett* **86** 4056–4059 (2001).

Kirkland EJ: Advanced Computing in Electron Microscopy. Plenum Press New York (1998).

Kisielowski C Freitag B Xu X Beckman SP Chrzan DC: Subangstrom imaging of dislocation core structures: how well are experiments comparable with theory? *Philos Mag* **86** 4575–4588 (2006).

Klie RF Buban JP Varela M Franceschetti A Jooss C *et al*: Enhanced current transport at grain boundaries in high-T_c superconductors. *Nature* **435** 475–478 (2005).

Kurata H Colliex C: Electron-energy-loss core-edge structures in manganese oxides. *Phys Rev B* **48** 2102–2108 (1993).

Kwon SY Kim HJ Yoon E Jang YD Yee KJ *et al*: Optical and microstructural studies of atomically flat ultrathin In-rich InGaN/GaN multiple quantum wells. *J Appl Phys* **103** Art. No. 063509 (2008).

Lakner H Bollig B Ungerechts S Kubalek E: Characterization of III-V semiconductor interfaces by Z-contrast imaging EELS and CBED. *J Phys D* **29** 1767–1778 (1996).

Lakner H Liu Q Brockt G Radefeld A Meinert A Scholz F: Investigation of inhomogeneities in (Al Ga In)N heterostructures by STEM and cathodoluminescence. *Mater Sci Eng B* **51** 44–52 (1998).

McGibbon MM Browning ND Chisholm MF McGibbon AJ Pennycook SJ *et al*: Direct determination of grain-boundary atomic-structure in $SrTiO_3$. *Science* **266** 102–104 (1994).

McGibbon MM Browning ND McGibbon AJ Pennycook SJ: The atomic structure of asymmetric [001] tilt boundaries in $SrTiO_3$. *Philos Mag A* **73** 625–641 (1996).

Mobus G Nufer S: Nanobeam propagation and imaging in a FEGTEM/STEM. *Ultramicroscopy* **96** 285 (2003).

Muller DA Shashkov DA Benedek R Yang LH Silcox J *et al*: Atomic scale observations of metal-induced gap states at 222MgO/Cu interfaces. *Phys Rev Lett* **80** 4741–4744 (1998).

Myhajlenko S Batstone JL Hutchinson HJ Steeds JW: Luminescence studies of individual dislocations in II–VI (ZnSe) and III–V (InP) semiconductors. *J Phys C* **17** 6477–6492 (1984).

Nellist PD Pennycook SJ: Incoherent imaging using dynamically scattered coherent electrons. *Ultramicroscopy* **78** 111–124 (1999).

Nellist PD Pennycook SJ: The principles and interpretation of annular dark-field Z-contrast imaging. In Advances in Imaging and Electron Physics (Eds. Kazan B Mulvey T Hawkes P) Elsevier New York 147–203 (2000).

Park WI Yi GC Kim MY Pennycook SJ: ZnO nanoneedles grown vertically on Si substrates by non-catalytic vapor-phase epitaxy. *Adv Mater* **14** 1841–1843 (2002).

Park WI Yi GC Kim M Pennycook SJ: Quantum confinement observed in ZnO/ZnMgO nanorod heterostructures. *Adv Mater* **15** 526–529 (2003).

Pauc N Phillips MR Aimez V Drouin D: Carrier recombination near threading dislocations in GaN epilayers by low voltage cathodoluminescence. *Appl Phys Lett* **89** (2006).

Peng YP Nellist PD Pennycook SJ: HAADF-STEM imaging with sub-angstrom probes: a full Bloch wave analysis. *J Electron Microsc* **53** 257–266 (2004).

Pennycook SJ: Studies of Cathodoluminescence on a Scanning Transmission Electron Microscope. Cavendish Laboratory University of Cambridge Cambridge (1978).

Pennycook SJ: Investigation of the electronic effects of dislocations by STEM. *Ultramicroscopy* **7** 99–104 (1981).

Pennycook SJ: Z-Contrast STEM for materials science. *Ultramicroscopy* **30** 58–69 (1989).

Pennycook SJ Berger SD Culbertson RJ: Elemental mapping with elastically scattered electrons. *J Microsc-Oxford* **144** 229–249 (1986).

Pennycook SJ Boatner LA: Chemically sensitive structure-imaging with a scanning-transmission electron-microscope. *Nature* **336** 565–567 (1988).

Pennycook SJ Brown LM: Cathodoluminescence at dislocations in divalent oxides. *J Lumin* **18**(9) 905–909 (1979).

Pennycook SJ Brown LM Craven AJ: Observation of cathodoluminescence at single dislocations by STEM. *Philos Mag A* **41** 589–600 (1980).

Pennycook SJ Browning ND McGibbon MM McGibbon AJ Jesson DE *et al*: Direct determination of interface structure and bonding with the scanning transmission electron microscope. *Philos Trans R Soc London Ser A* **354** 2619–2634 (1996).

Pennycook SJ Jesson DE: High-resolution incoherent imaging of crystals. *Phys Rev Lett* **64** 938–941 (1990).

Pennycook SJ Jesson DE: High-resolution Z-contrast imaging of crystals. *Ultramicroscopy* **37** 14–38 (1991).

Pennycook SJ Jesson DE: Atomic resolution Z-contrast imaging of interfaces. *Acta Metall Mater* **40** S149–S159 (1992).

Pennycook SJ Narayan J: Direct imaging of dopant distributions in silicon by scanning-transmission electron-microscopy. *Appl Phys Lett* **45** 385–387 (1984).

Pennycook SJ Nellist PD: Z-contrast scanning transmission electron microscopy. In Impact of Electron and Scanning Probe Microscopy on Materials Research (Eds. Rickerby DG Valdré U Valdré G) Kluwer Academic Publishers Dordrecht The Netherlands 161–207 (1999).

Petroff PM Lang DV: New spectroscopic technique for imaging spatial-distribution of nonradiative defects in a scanning-transmission electron-microscope. *Appl Phys Lett* **31** 60–62 (1977).

Petroff PM Logan RA Savage A: Nonradiative recombination at dislocations in III–V compound semiconductors. *J Microsc-Oxford* **118** 255–261 (1980a).

Petroff PM Logan RA Savage A: Nonradiative recombination at dislocations in III–V compound semiconductors. *Phys Rev Lett* **44**:287–291 (1980b).

Petroff PM Weisbuch C Dingle R Gossard AC Wiegmann W: Luminescence properties of GaAs–$GA_{1-X}AL_X$ As double heterostructures and multiquantum-well superlattices grown by molecular-beam epitaxy. *Appl Phys Lett* **38** 965–967 (1981).

Piqueras J Llopis J Delgado L: Cathodoluminescence from defects in indented MgO. *J Appl Phys* **52** 4341–4344 (1981).

Ponce FA Bour DP Gotz W Wright PJ: Spatial distribution of the luminescence in GaN thin films. *Appl Phys Lett* **68** 57–59 (1996).

Ponce FA Srinivasan S Bell A Geng L Liu R *et al*: Microstructure and electronic properties of InGaN alloys. *Phys Status Solidi B* **240** 273–284 (2003).

Rafferty B Nellist PD Pennycook SJ: On the origin of transverse incoherence in Z-contrast STEM. *J Electron Microsc* **50** 227–233 (2001).

Smith DJ: The realization of atomic resolution with the electron microscope. *Rep Prog Phys* **60** 1513–1580 (1997).

Smith DJ: Progress and perspectives for atomic-resolution electron microscopy. *Ultramicroscopy* **108** 159–166 (2008).

Steyn JB Giles P Holt DB: Efficient spectroscopic detection system for cathodoluminescence mode scanning electron-microscopy (SEM). *J Microsc-Oxford* **107** 107–128 (1976).

Strunk HP Albrecht M Scheel H: Cathodoluminescence in transmission electron microscopy. *J Microsc-Oxford* **224** 79–85 (2006).

Sutton AP: Irrational tilt grain-boundaries as one-dimensional quasicrystals. *Acta Metall* **36** 1291–1299 (1988).

Sutton AP Vitek V: On the structure of tilt grain-boundaries in cubic metals. 1. Symmetrical tilt boundaries. *Philos Trans R Soc A* **309** 1–68 (1983).

Taylor WE Odell NH Fan HY: Grain boundary barriers in germanium. *Phys Rev* **88** 867 (1952).

Treacy MMJ: Imaging with Rutherford scattered electrons in the scanning-transmission electron-microscope. *Scanning Electron Microscopy* 185–197 (1981).

Treacy MMJ: Optimizing atomic-number contrast in annular dark field images of thin-films in the scanning-transmission electron-microscope. *J Microsc Spect Elec* **7** 511–523 (1982).

Treacy MMJ Howie A Pennycook SJ: Z-contrast of supported catalyst particles on the STEM. In Electron Microscopy and Analysis 1979 (Ed. Mulvey T) Institute of Physics Brighton 261–266 (1980).

Treacy MMJ Howie A Wilson CJ: Z-contrast of platinum and palladium catalysts. *Philos Mag A* **38** 569–585 (1978).

Varela M Findlay SD Lupini AR Christen HM Borisevich AY *et al*: Spectroscopic imaging of single atoms within a bulk solid. *Phys Rev Lett* **92** Art. No. 095502 (2004).

Velednitskaya MA Rozhanskii VN Comolova LF Saparin GV Schreiber J *et al*: Investigation of deformation mechanism of MgO crystals affected by concentrated load. *Phys Status Solidi A* **32** 123– (1975).

Vollman M Waser R: Grain-boundary defect chemistry of acceptor-doped titanates—space-charge layer width. *J Am Ceram Soc* **77** 235–243 (1994).

Wall J Langmore J Isaacson M Crewe AV: Scanning-transmission electron-microscopy at high-resolution. *Proc Natl Acad Sci USA* **71** 1–5 (1974).

Williams PM Yoffe AD: Scanning electron microscope studies of cathodoluminescence in ZnSe single crystals. *Philos Mag* **18** 555–560 (1968).

Xin Y James EM Arslan I Sivananthan S Browning ND *et al*: Direct experimental observation of the local electronic structure at threading dislocations in metalorganic vapor phase epitaxy grown wurtzite GaN thin films. *Appl Phys Lett* **76** 466–468 (2000a).

Xin Y James EM Browning ND Pennycook SJ: Atomic resolution Z-contrast imaging of semiconductors. *J Electron Microsc* **49** 231–244 (2000b).

Xin Y Pennycook SJ Browning ND Nellist PD Sivananthan S *et al*: Direct observation of the core structures of threading dislocations in GaN. *Appl Phys Lett* **72** 2680–2682 (1998).

Yacobi BG Datta S Holt DB: Form of edge emission band in CdS and ZnS crystals. *Philos Mag* **35** 145–158 (1977).

Yacobi BG Holt DB: Cathodoluminescence scanning electron-microscopy of semiconductors. *J Appl Phys* **59** R1–R24 (1986).

Yacobi BG Holt DB: Cathodoluminescence Microscopy of Inorganic Solids. Plenum New York (1990).

Yamamoto N Itoh H Grillo V Chichibu SF Keller S *et al*: Cathodoluminescence characterization of dislocations in gallium nitride using a transmission electron microscope. *J Appl Phys* **94** 4315–4319 (2003).

Yamamoto N Spence JCH Fathy D: Cathodoluminescence and polarization studies from individual dislocations in diamond. *Philos Mag B* **49** 609–629 (1984).

Yan Y Chisholm MF Duscher G Maiti A Pennycook SJ *et al*: Impurity-induced structural transformation of a MgO grain boundary. *Phys Rev Lett* **81** 3675–3678 (1998).

Yuan J Berger SD Brown LM: Thickness dependence of cathodoluminescence in thin-films. *J Phys* **1** 3253–3265 (1989).

Zaldivar MH Fernandez P Piqueras J: Study of defects in GaN films by cross-sectional cathodoluminescence. *J Appl Phys* **83** 2796–2799 (1998).